*Journal of Zhejiang University-SCIENCE A (Applied Physics & Engineering)* 2022 23(2):140-155
www.jzus.zju.edu.cn; www.springer.com/journal/11582
E-mail: jzus_a@zju.edu.cn

**Research Article**

https://doi.org/10.1631/jzus.A2100222



# Experimental and theoretical study on the break phenomenon of self-pulsation for liquid-centered swirl coaxial injectors

Peng-jin CAO, Xiao BAI✉, Qing-lian LI✉, Peng CHENG

*Science and Technology on Scramjet Laboratory, College of Aerospace Science and Engineering,National University of Defense Technology, Changsha 410073, China*

**Abstract:** Experimental observations together with theoretical analysis were conducted to investigate the break phenomenon and the corresponding mechanisms of self-pulsation for a liquid-centered swirl coaxial injector with recess number of RN=1. Instantaneous spray images were obtained based on background light imaging technology with a high-speed camera. By dynamic analysis of the flow process of the liquid sheet in the recess chamber, a 1D self-pulsation theoretical model was established, and the self-sustaining mechanisms of self-pulsation were analyzed in depth. The results show that the increase of the momentum flux ratio will lead to the occurrence of the break phenomenon of self-pulsation for the injector with a larger recess length, and the frequency and intensity of self-pulsation before and after the break phenomenon differ significantly. The flow dynamics in the recess chamber sequentially transform from a periodic expansion-dominated flow to a stable flow, and then develop to a periodic contraction-dominated flow during the break process of self-pulsation. With the occurrence of self-pulsation before the break phenomenon, the liquid sheet has little effect on the pressure disturbance in the recess chamber. In contrast, with the occurrence of self-pulsation after the break phenomenon, the pressure disturbance is obviously affected by the liquid sheet. Based on the theoretical analysis model of self-pulsation, the self-pulsation frequency can be predicted. Furthermore, the self-sustaining mechanism of self-pulsation before and after the break phenomenon is preliminarily confirmed. The energy transfer between the gas- and liquid-phase is an important factor for maintaining the self-pulsation process.

**Key words:** Break phenomenon; Theoretical model of self-pulsation; Pressure oscillation characteristics; Recess; Liquid-centered swirl coaxial (LCSC) injector

## 1 Introduction

As the main power source of energy devices for space applications, liquid-fuel rocket engines are widely used in the first stage of most carrier rockets due to their high specific impulse, large thrust, and adjustable thrust system (Gomet et al., 2014). The atomization and mixing processes of the propellants are completed by an injector, after which the propellants evaporate and burn. Therefore, the injector is crucial for the stable operation of such engines (Yang and Fu, 2011; Armbruster et al., 2020). Liquid-centered swirl coaxial (LCSC) injectors are characterized by good atomization, mixing, and combustion performance, and are widely used (Fu et al., 2011; Kim JG et al., 2013; Kim YJ et al., 2014; Li et al., 2017; Giannadakis et al., 2019), e.g. Russia's RD-57 engine and China's YF-73 and YF-75 engines. This type of injector easily experiences self-pulsation under certain structural and operating conditions (Im et al., 2009; Bai et al., 2020b), and the self-pulsation frequency is between 1 and 10 kHz, which is accompanied by a serious acoustic scream (Kang et al., 2018).

Self-pulsation was first identified in the LCSC injector used in the $LO_x/H_2$ propulsion system developed by the former Soviet Union in the 1970s (Bazarov and Yang, 1998). Spray self-pulsation will cause the oscillation of the pressure and mass flow, which will inevitably lead to the oscillation of the atomization and combustion processes. Moreover, the acoustic scream caused by self-pulsation may be coupled with the acoustic characteristics of the

✉ Xiao BAI, zndxbx@163.com
Qing-lian LI, peakdreamer@163.com
Peng-jin CAO, https://orcid.org/0000-0002-5937-3181

Received May 13, 2021; Revision accepted Aug. 3, 2021;
Crosschecked Dec. 31, 2021

combustor and ultimately produce unstable combustion (Yuan and Shen, 2016; Armbruster et al., 2018). Bazarov and Yang (1998) summarized the causes and studied the influencing factors of self-pulsation; they found that self-pulsation can be weakened or eliminated by significantly increasing or reducing the recess length of the inner post of the injector, increasing the size of the annular gap, and dispersing the place of liquid flow impingement with a gaseous stream. Kang et al. (2016a) and Ren et al. (2021a, 2021b) experimentally and numerically studied the influence of the recess length on self-pulsation and categorized the flow modes in the recess chamber as external mixing, critical mixing, and internal mixing. They reported that self-pulsation is the strongest when flow is around the critical mixing flow. Bai et al. (2020b) experimentally investigated the relationship between self-pulsation, flame oscillation, and combustion instability, and indicated that the flame and supply system produce the same frequency oscillation during the occurrence of self-pulsation. In addition, when the self-oscillation frequency and the first-order natural longitudinal frequency of the combustor are coupled, combustion instability will be excited. Im and Yoon (2013) showed that the important geo-metrical parameters that affect self-pulsation include the recess length of the inner post, the annulus width, and the size of the air core of the swirl injector; while the operating parameters that affect self-pulsation include the gas-liquid phase velocity, the mass flow rate, the gas-liquid phase momentum ratio, the fluid properties, and the backpressure. Im and Yoon (2013) confirmed that the self-pulsation frequency is proportional to the Reynolds numbers of both the gas and liquid, but is mainly controlled by the Reynolds number of the liquid. Self-pulsation can reduce the spray quality, and its frequency is consistent with the frequency of the liquid sheet surface wave. Bai et al. (2019) and Chu et al. (2021) experimentally and numerically studied the influence of the backpressure on the spray and proposed that backpressure can change the flow of the liquid sheet in the recess chamber to enhance or weaken the blocking effect of the conical liquid sheet on the gas, thereby affecting the self-pulsation and spray cone angle. With the increase of backpressure, the spray changes from a self-pulsated state to a stable state, and the spray cone angle first increases and then decreases.

The recess length is one of the key structural parameters of self-pulsation (Kim et al., 2007b; Yang et al., 2008; Ahn et al., 2014; Li et al., 2016; Ranade and Frederick, 2019), but the mechanism of its effect on self-pulsation remains unclear. Huang et al. (1998) believed that self-pulsation is the result of the oscillation of the annular gas on the outlet wall of the inner injector and the natural frequency of the central gas core resonance. Im et al. (2009) found that the oscillation frequency of the liquid sheet surface wave is consistent with the self-pulsation frequency, and posited that the oscillation of the liquid sheet surface wave is the cause of self-pulsation. Kang et al. (2016b) and Eberhart and Frederick Jr (2017a, 2017b) believed that self-pulsation is related to the Kelvin-Helmholtz (K-H) instability at the gas-liquid interface, and that self-pulsation will occur when the K-H vortex energy is sufficient to overcome the inertia of the liquid. Bai et al. (2018) posited that the periodic blockage effect of the liquid sheet in the recess chamber is the decisive factor that causes self-pulsation of the LCSC injector. Previous studies have shown that the break phenomenon of self-pulsation will occur for the LCSC injectors with a larger recess length (Bai, 2020). In other words, with the increase of the gas mass flow rate, the spray will change from the self-pulsated state to the stable state, and then back to the self-pulsated state. Moreover, self-pulsation before and after the break phenomenon is considered to be dominated by different mechanisms (Bai, 2020).

It has been determined that the break phenomenon of self-pulsation greatly influences the atomization and combustion properties of the liquid-fuel rocket engine. However, research on the spray characteristics before and after the break phenomenon, as well as on the dominant mechanisms, is preliminary. In the present study, the pressures at different axial positions inside the recess chamber were measured and analyzed using high-frequency pressure sensors. An observation of the spray pattern with varying momentum flux ratios ($J$) was undertaken. Experiments with a transparent injector were performed to investigate the flow modes of the break phenomenon in the recess chamber. Theoretical analysis was carried out to study the liquid sheet's motion rule in the recess chamber. A

theoretical model of self-pulsation was established to predict the self-pulsation frequency and further reveal the self-sustaining mechanisms of self-pulsation before and after the break phenomenon.

## 2 Experimental

### 2.1 Experimental facilities

The experimental system consisted of a propellant supply system, an LCSC injector, a spray collector, a Photron FASTCAM SA-X2 camera (Japan), and a Aertai (ART) data acquisition system (China). As shown in Fig. 1, a cold non-contact spray test was conducted at atmospheric pressure with filtered water and dry air as the simulation media. Data on the pressures of the liquid- and gas-collecting chamber were collected with piezoelectric pressure sensors, the measurement accuracy of which was 0.5% full scale (FS). The liquid mass flow rate was measured by a turbine flow meter, the measurement accuracy of which was 0.5% FS. Moreover, data on the gas temperatures and pressures were measured to calculate the volume flow rate of the gas simulation medium.

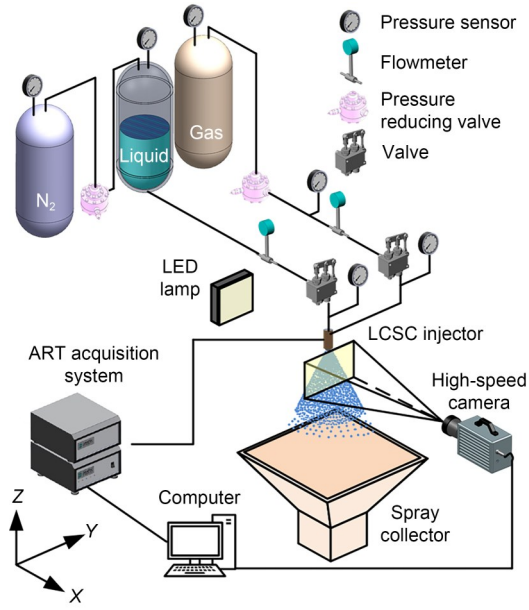


**Fig. 1 Experimental system (LED: light emitting diode)**

The LCSC injector used in the test is shown in Fig. 2. It includes an internal swirl injector and an external annular gap. The key structural parameters are reported in Table 1. The liquid enters the swirl chamber through four tangential holes uniformly arranged in the circumferential direction, and is then ejected with a conical liquid sheet after traveling through the contraction section and the straight section. The atomization process is completed via interaction with the annular gas injected into the recess chamber at high speeds. To observe the flow process in the recess chamber, an external quartz glass nozzle, a high-speed camera, a small pressure sensor, and an external metal nozzle were used to carry out the experiments.

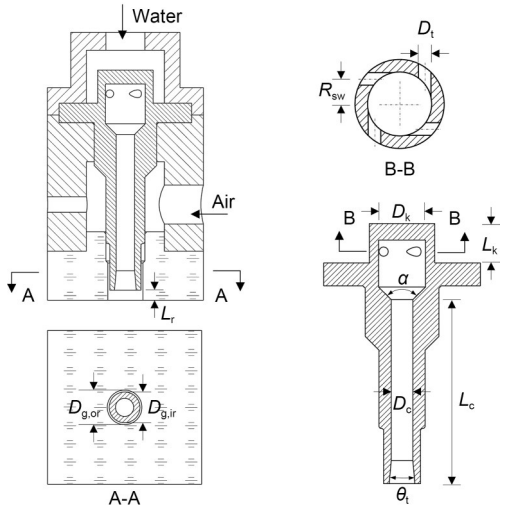


**Fig. 2 Schematic diagram of the LCSC injector**

**Table 1 Geometric parameters of the LCSC injector**

| Parameter | Value |
|---|---|
| Nozzle diameter, $D_c$ (mm) | 4.7 |
| Length of straight section, $L_c$ (mm) | 40.05 |
| Inner diameter of annular gap, $D_{g,ir}$ (mm) | 8 |
| Outer diameter of annular gap, $D_{g,or}$ (mm) | 9 |
| Diameter of swirl chamber, $D_k$ (mm) | 10.2 |
| Length of swirl chamber, $L_k$ (mm) | 10.2 |
| Diameter of tangential hole, $D_t$ (mm) | 2 |
| Swirl radius of liquid flow, $R_{sw}$ (mm) | 4 |
| Contract angle, $\alpha$ (°) | 90 |
| Expansion angle, $\theta_t$ (°) | 10 |
| Recess length, $L_r$ (mm) | 8 |

### 2.2 Experimental conditions

The test conditions are reported in Table 2. The liquid mass flow rate was kept constant, and the gas mass flow rate was varied within a certain range according to the flow characteristics in the recess chamber. The deviations of the gas and liquid

mass flow rates were less than 2% and 4%, respectively. The recess number (RN) is defined as a dimensionless parameter, which divides the recess length ($L_r$) by the inner diameter of the oxidizer post ($D_{g,ir}$), RN=$L_r/D_{g,ir}$.

### 2.3 Experimental techniques

Background light imaging technology was used to capture transient images of the self-pulsated spray and the recess chamber. It included the use of a high-speed camera (Photron FASTCAM SA-X2) and a surface light source (Opt-APA3024-2). The exposure time of the camera was set at 50 μs, the sizes of the transient spray images were 1024×512, and the frame rate was set as 20 000 frames/s. The spray oscillation frequency was obtained by processing the transient spray images. Firstly, the raw images, with and without spray, were used to subtract the background and converted to gray images. Secondly, an appropriate threshold was selected to transform the gray images into binary images. Thirdly, the spray width was obtained based on a measurement line placed at $1.5D_{g,or}$ distance from the injector face. Finally, applying the three steps to 2000 instantaneous self-pulsated spray images obtained a time series of the spray width, and then the frequency and intensity of the spray width were obtained via the fast Fourier transform (FFT) of the time series of the spray width.

A high-frequency pressure sensor (Model XCQ-80-7BARA, Kulite Semiconductor Products, the USA) was used to determine the pressure oscillation in the recess chamber. The electrical signal output from the high-frequency pressure transducer was collected by the ART acquisition system at a sampling frequency of 1024 kHz and a sampling period of 3 s.

## 3 Results and discussion

### 3.1 Break phenomenon of self-pulsation

The development of the surface wave of liquid sheet, the oscillations of the annular gas and gas core, and the gas-liquid interaction in the recess chamber lead to a complicated spray formation (Kim et al., 2007a). Shear forces between both propellants lead to an instability of the liquid jet and finally to a disintegration into ligaments and droplets (Lux and Haidn, 2009). Therefore, atomization characterizing dimensionless numbers such as the momentum flux ratio $J$ ($J=(\rho v^2)_g/(\rho v^2)_l$) take into account the relative motion of the two fluids. Fig. 3 presents the spray images and frequency spectra of the LCSC injector under different conditions with RN=1, from which it can be seen that the spray pattern changes significantly with the increase in $J$. As depicted in Fig. 3a, the spray pattern shows a more stable cone under low $J$ ($J$=1.05), and with the increase of $J$ ($J$=3.14), self-pulsation occurs and forms a Christmas-tree-like shape (Fig. 3b), after which the spray transforms to a stable state ($J$=8.90), as plotted in Fig. 3c. At that time, the high gas injection velocity increases the droplet velocity outside the liquid sheet, and the spray exhibits fuzzy boundaries. However, the spray width is relatively stable and the spray angle stays nearly constant due to the stable gas-liquid shear layer. Finally, self-pulsation occurs again under high $J$ ($J$=12.48), as shown in Fig. 3d. At this time, the turbulence of the spray is greatly strengthened, and asymmetric distribution of the spray occurs on the outer edge of the liquid sheet in vortexes of different scales (Ranade and Frederick, 2019). The spray width at the stable state is found to remain almost constant on the same section perpendicular to the injection faceplate.

**Table 2 Experimental conditions and parameters**

| Test No. | $\Delta p_l$ (MPa) | $\dot{m}_l$ (g/s) | $\Delta p_g$ (MPa) | $\dot{m}_g$ (g/s) | $J$ | RN | Test equipment |
|---|---|---|---|---|---|---|---|
| 1 | 0.65 | 160 | 0.038 | 2.4 | 1.05 | 1 | High-speed camera, high-frequency pressure transducer |
| 2 | 0.65 | 160 | 0.114 | 5.3 | 3.14 | 1 | |
| 3 | 0.65 | 160 | 0.303 | 11.0 | 6.42 | 1 | |
| 4 | 0.65 | 160 | 0.494 | 15.3 | 8.90 | 1 | |
| 5 | 0.65 | 160 | 0.673 | 20.2 | 11.51 | 1 | |
| 6 | 0.65 | 160 | 0.739 | 22.8 | 12.48 | 1 | |
| 7 | 0.65 | 160 | 0.973 | 28.8 | 17.04 | 1 | |
| 8 | 0.65 | 160 | 1.400 | 41.2 | 22.55 | 1 | |
| 9 | 0.65 | 160 | 1.790 | 51.0 | 27.23 | 1 | |

$\Delta p_l$ is the liquid pressure drop, $\Delta p_g$ is the gas pressure drop, $\dot{m}_l$ is the liquid mass flow rate, and $\dot{m}_g$ is the gas mass flow rate

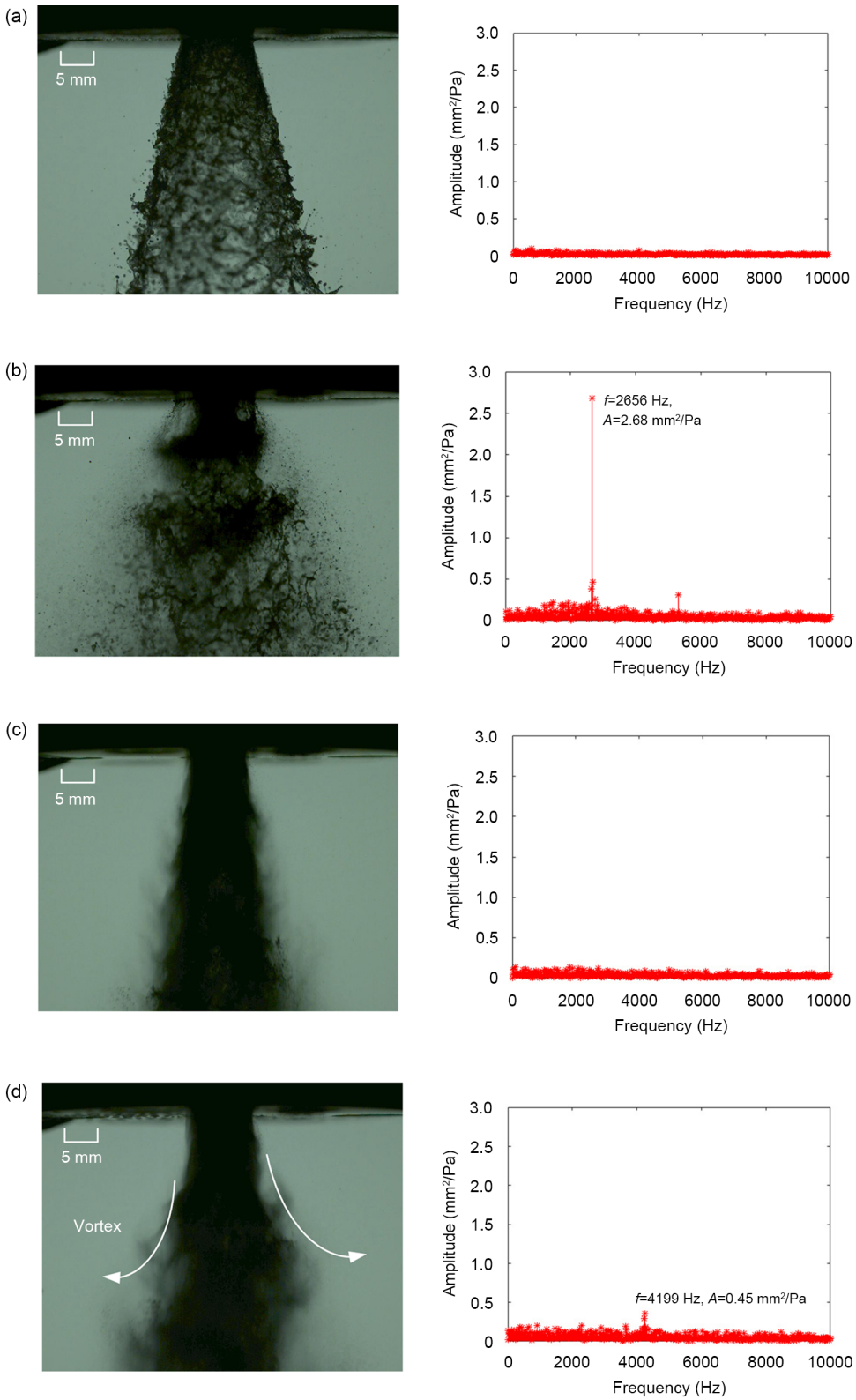


**Fig. 3 Instantaneous spray images and frequency spectra: (a) steady spray, $J$=1.05, $Re_g$=10 085.95; (b) self-pulsated spray, $J$=3.14, $Re_g$=22 411.65; (c) steady spray, $J$=8.90, $Re_g$=64 123.49; (d) self-pulsated spray, $J$=12.48, $Re_g$=89 296.23. $f$ is the self-pulsation frequency, $A$ is the self-pulsation amplitude, and $Re_g$ is the gas Reynolds number. Reprinted from (Bai et al., 2021), Copyright 2021, with permission from Elsevier**

However, the self-pulsated spray width oscillates periodically. Fig. 4 shows the variations of the spray width oscillation frequency and intensity with *J*. According to the findings, the dark blue regions in the figure represent the stable-spray area, and the latter stable-spray region represents the zone of the break phenomenon of self-pulsation. Before the occurrence of break phenomenon, the self-pulsation frequency is nearly unchanged, but after the disappearance of break phenomenon it decreases slightly.

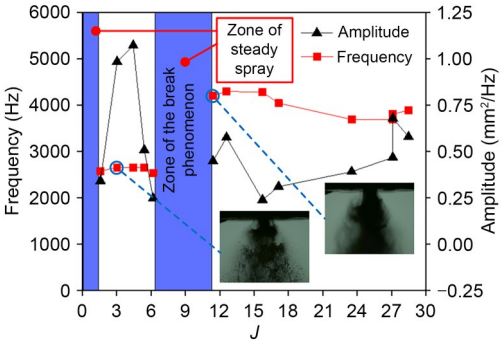


**Fig. 4 Variations of the frequency and amplitude of self-pulsation with *J*. References to color refer to the online version of this figure**

Overall, the self-pulsation frequency after the break phenomenon is 1500 Hz higher than that before it. This is because, before the break phenomenon, the force of the annular gas on the liquid sheet is weak due to the low gas momentum. Moreover, the liquid sheet is characterized by a long radial movement distance. After the break phenomenon, the gas has higher momentum. The annular gas exerts a strong force on the liquid sheet, which greatly limits the radial movement of the liquid sheet in the recess chamber. Furthermore, the radial movement distance of the liquid sheet in a period is reduced, the initial radial velocity of the liquid sheet remains nearly unchanged, and the time in which the liquid sheet moves within a period is reduced. Thus, the self-pulsation frequency increases after the break phenomenon compared with that before the break phenomenon.

## 3.2 Characteristics of pressure oscillation in the recess chamber

### 3.2.1 Self-sustaining mechanism of self-pulsation

The recess length is considered as one of the most crucial factors that influence the spray pattern of the LCSC injector. Both Kang et al. (2016a) and Bai et al. (2018) explored the influences of the recess length on the self-pulsated spray, and found that the spray transforms from a stable state to a self-pulsated state with the increase of the recess length. The variation of the recess length affects the gas-liquid interaction process, which leads to the transformation of the spray pattern. The physical process of the breaking and atomization of the strongly swirling liquid sheet after its collision with the annular gas in the recess chamber is very complex. Thus, the pressure oscillation time series of the self-pulsated state, monitored by the high-frequency pressure sensor on the recess chamber wall, are used as a reference, and four moments within an oscillation period are selected as the research object. The moments of concern and the corresponding pressure positions are shown in Fig. 5.

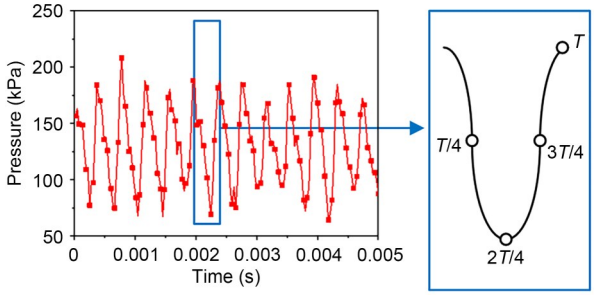


**Fig. 5 Distribution of the moments of concern within an oscillation period**

Four typical working conditions are selected to analyze the liquid flow dynamics in the recess chamber. As shown in Fig. 6, due to the influence of the refraction of quartz glass, black streaks inevitably appear in the images. However, the shape of the liquid sheet is still clearly visible. The white dashed line in the figure indicates the boundary between the recess chamber and the annular gap. When *J* is extremely low (*J*= 1.05), the spray state is stable, and the liquid sheet in the recess chamber also shows a stable cone, as shown in Fig. 6c. With the increase of *J* (*J*=3.14), a self-pulsated spray appears. At that time, due to the low gas-liquid momentum ratio, the gas-liquid interaction is weak, and the liquid sheet continues to squeeze the gas, which reduces the gas circulation area. Moreover, the gas pressure outside the liquid sheet increases, which increases the force preventing the liquid sheet from approaching the recess chamber wall. The radial velocity of the liquid sheet decreases rapidly until the

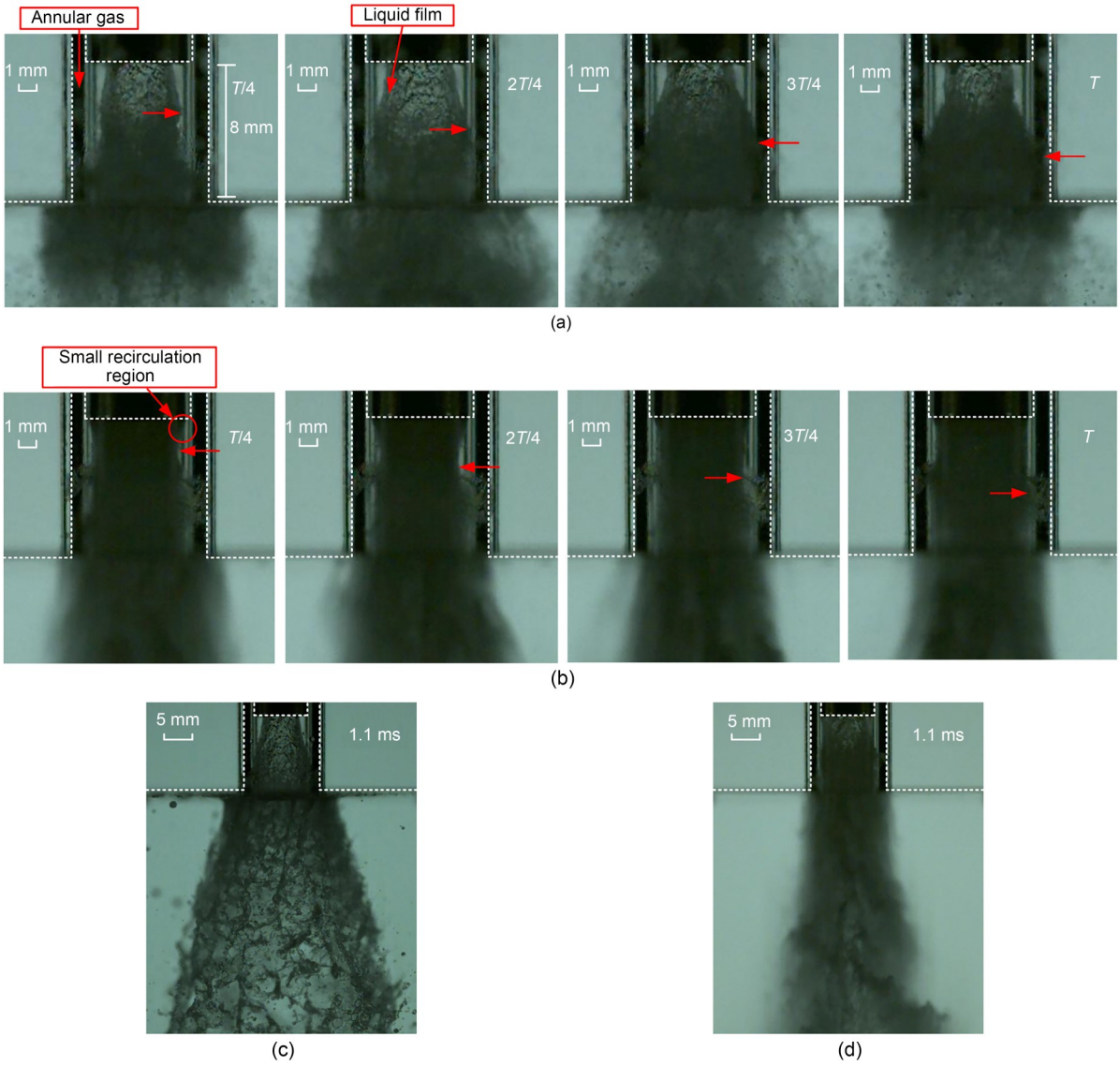


**Fig. 6 Liquid sheet flow pattern in the recess chamber under typical working conditions: (a) self-pulsated spray before the break phenomenon; (b) self-pulsated spray after the break phenomenon; (c) steady spray at minimal *J*; (d) steady spray under the break phenomenon**

liquid sheet hits the recess chamber wall or the radial velocity decreases to zero, after which it increases in the opposite direction. The liquid sheet then moves toward the centerline of the injector, the gas circulation area continues to increase, the gas pressure outside the liquid sheet decreases rapidly, and the resultant force of the liquid sheet drives the liquid sheet closer to the recess chamber wall. This reciprocating gas-liquid interaction causes the spray width to oscillate periodically.

The self-pulsated spray at this time is thought to be caused by a periodic blocking of the annular gas channel by the liquid sheet, as indicated by the light arrow in Fig. 6a. At a medium $J$ ($J$=8.90), the spray transforms from the self-pulsated state to the stable state, and the shape of the liquid sheet in the recess chamber has changed little, as shown in Fig. 6d. At that time the gas-liquid shear layer is relatively stable and the gas channel is directly connected to the outer atmosphere. Consequently, the gas-liquid interaction in the recess chamber occurs in a relatively balanced state. At high $J$ ($J$=12.48), the self-pulsated spray appears again. As shown in Fig. 6b, many small droplets that are stripped off the liquid sheet by the gas

injected at high speed fill up the small recirculation area at the outlet wall of the inner nozzle and blur the gas-liquid interface. However, the movement process of the liquid sheet can still be distinguished. Under high-momentum gas injection, the liquid sheet is squeezed to move toward the centerline of the injector, thereby increasing the pressure of the gas core inside the liquid sheet. Simultaneously, the pressure outside the liquid sheet decreases, and the resultant force of the liquid sheet stops it from moving to the centerline of the injector. Finally, the gas pressure outside the liquid sheet squeezes it toward the centerline again, after which it returns to the recess chamber wall. The self-pulsated spray at this time is thought to be caused by the periodic squeezing of the liquid sheet by the annular gas.

### 3.2.2 Pressure oscillation in the recess chamber

When self-pulsation occurs, the pressure outside the liquid sheet in the recess chamber oscillates periodically, at a frequency the same as that of the spray width (Bai et al., 2020b). Therefore, the periodic change of the liquid sheet in the recess chamber is the direct cause of the pressure oscillation in the recess chamber (Chu et al., 2020). Fig. 7 presents the pressure oscillation time series and frequency spectrum in the recess chamber under the four typical working conditions.

If the self-pulsated spray appears before the break phenomenon ($J$=3.14), the annular gas channel in the recess chamber is blocked by the liquid sheet. The gas-liquid interaction is relatively weak with a self-pulsation frequency of 2507 Hz. The pressure outside the liquid sheet rises, and the peak pressure reaches 0.215 MPa, which is about 212% of standard atmospheric pressure. When the high pressure outside the liquid sheet in the recess chamber stops the liquid sheet from moving to the recess chamber wall and causes it to reverse to the injector centerline, the gas channel opens, the pressure decreases, and the minimum pressure value is 0.02 MPa, which is about 20% of standard atmospheric pressure, as shown in Fig. 7b. When the spray state is stable ($J$=1.05, 8.90), the pressure in the recess chamber and the spray width oscillation exhibit no obvious dominant frequency. At this time, the pressure value is stable and tends to 0.12 MPa, which is close to atmospheric pressure, as shown in Figs. 7a and 7c.

For the self-pulsated spray after the break phenomenon ($J$=12.48), the self-pulsation frequency

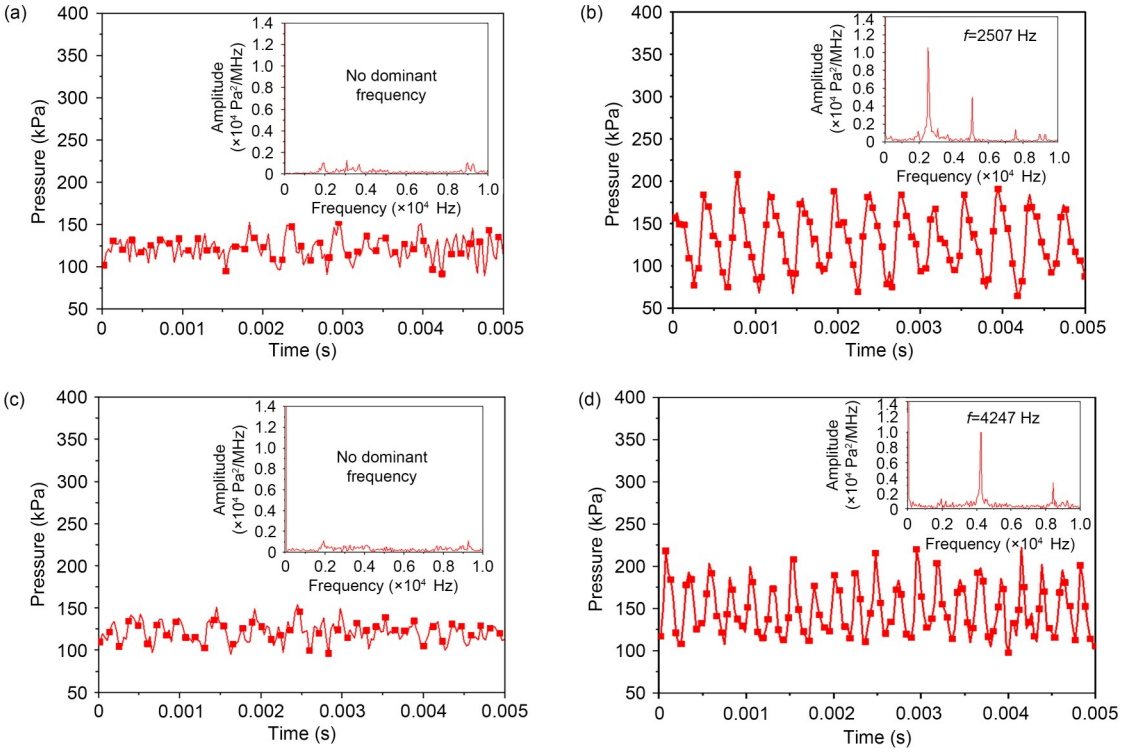


**Fig. 7 Pressure time series and frequency spectrum in the recess chamber: (a) $J$=1.05; (b) $J$=3.14; (c) $J$=8.90; (d) $J$=12.48**

becomes 4247 Hz due to violent gas-liquid interaction in the recess chamber. The high-momentum gas first squeezes the liquid sheet to move toward the centerline of the injector, the gas pressure on the recess chamber wall decreases, and the minimum pressure value is 0.085 MPa. When the gas pressure outside the liquid sheet is less than a certain critical value, the liquid sheet moves to the recess chamber wall, which increases the gas pressure; at that time, the peak pressure is 0.22 MPa, as shown in Fig. 7d. The analysis indicates that the peak pressure oscillation in the recess chamber caused by the self-pulsated spray is higher after the break phenomenon than that before the break phenomenon, but its oscillation amplitude is lower than that before the break phenomenon. This is because as the momentum of the gas injection increases, the force hindering the movement of the liquid sheet increases, and the amplitude of the liquid sheet movement in the radial direction decreases.

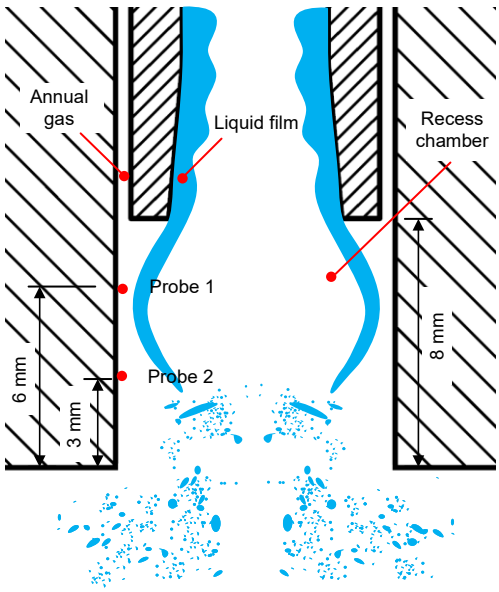


**Fig. 8 Locations of monitoring points. Reprinted from (Bai et al., 2021), Copyright 2021, with permission from Elsevier**

3.2.3 Pressure disturbance in the recess chamber

For the LCSC injector with RN=1, two high-frequency pressure detection points are set in the recess chamber, as shown in Fig. 8. Monitoring points 1 and 2 are located on different axial positions in the recess chamber; monitoring point 1 is 6 mm away from the injection faceplate, while monitoring point 2 is 3 mm away from the injection faceplate. A Kulite sensor is used to collect high-frequency pressure data, and the pressure distributions of the recess chamber at different monitoring points before, during, and after the break phenomenon are obtained, as shown in Fig. 9. The analysis reveals that when the self-pulsated spray appears before the break phenomenon ($J$=3.14), the annular gas pressure in the recess chamber decreases along the flow direction. This is because the gas is blocked by the liquid sheet at the outlet of the annular joint, and the gas-liquid interaction becomes intense, which causes a certain pressure loss. The pressure loss from monitoring point 1 to monitoring point 2 is about 10 kPa.

The analysis of the four cycles from 0.0030 to 0.0045 s reveals that there is almost no phase difference between the pressure curves of the two monitoring points, as presented in Fig. 9a. It indicates that the propagation speed of the pressure disturbance is very fast under this working condition, and that the liquid sheet has little effect on the disturbance. After the break phenomenon ($J$=12.48), the self-pulsated spray causes the annular gas pressure in the recess chamber to increase along the flow direction. This is because the gas at the outlet of the annular joint acts on the liquid sheet, which causes the liquid sheet to instantaneously have higher energy. Then the high-energy liquid sheet continuously blocks the low-energy gas near the injection faceplate in the recess chamber, causing continuing increase in the gas pressure. Analysis of the pressure curves of the two monitoring points of the recess chamber under this working condition indicates that the pressure disturbance in the recess chamber propagates down-stream from the outlet of the annular gap, but the propagation speed is obviously affected by the liquid sheet. There is a 12% phase difference between the pressure time series of the two monitoring points, as shown in Fig. 9c.

It is worth noting that with the occurrence of the break phenomenon of self-pulsation, the pressure amplitudes outside the liquid sheet in the recess chamber still reach approximately 25% of the average condition, which may give rise to combustion instability. With the increase of $J$ from 7.30 to 8.90, the high-pressure area in the recess chamber gradually changes from monitoring point 1 to monitoring point 2, as shown in Fig. 9b.

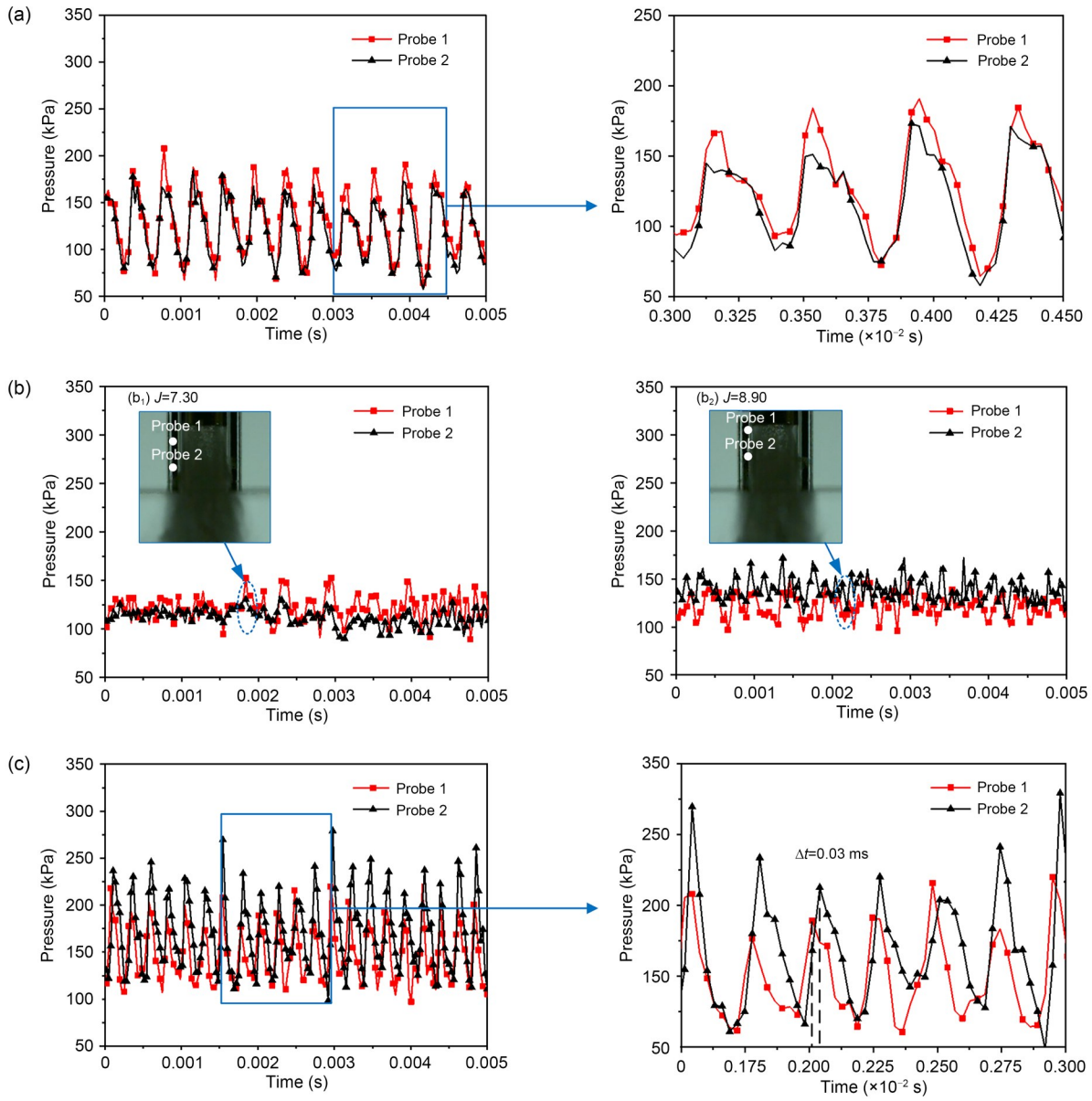


**Fig. 9 Pressure time series at different positions on the recess chamber wall: (a) self-pulsated spray before the break phenomenon (*J*=3.14); (b) steady spray during the break phenomenon (*J*=7.30 and 8.90); (c) self-pulsated spray after the break phenomenon (*J*=12.48)**

### 3.3 Theoretical analysis model for self-pulsation

Experimental studies show that when self-pulsation occurs, the movement of the liquid sheet in the recess chamber is closely related to the pressure of the annular gas channel. During self-pulsation, the interaction between the annular gas and the conical liquid sheet is in an unstable state. Therefore, by taking the liquid sheet element as the analysis object, a 1D unsteady analysis of the movement trajectory of the liquid sheet and the annular gas pressure in the LCSC injector with RN=1 is carried out. The oscillation period, the time series of the gas pressure outside the liquid sheet in the recess chamber, and the trajectory of the liquid sheet in the recess chamber are determined by theoretical calculation. Then the theoretical analysis and calculation results are compared with the experimental results to verify the practicality and feasibility of the theoretical model.

To simplify the analysis, the assumptions are as follows:

(1) The liquid phase is incompressible and inviscid;

(2) The energy loss in the flow process is neglected;

(3) The static pressure difference between the upstream and downstream of the liquid sheet is ignored;

(4) The volume force is not considered;

(5) The total pressure loss in the gas phase is ignored.

According to assumptions (1) and (4), the liquid sheet elements in the recess chamber are mainly subjected to the gas pressure inside and outside the liquid sheet, centrifugal force, and surface tension (Chen and Yang, 2014). Among them, the centrifugal force and the gas pressure inside the liquid sheet cause the liquid sheet to expand outward, and the surface tension and the gas pressure outside the liquid sheet cause the liquid sheet to contract inward. Numerical simulation studies have found that when self-pulsation occurs, the amplitude of pressure oscillation inside the liquid sheet is much lower than that outside the liquid sheet (Bai, 2020). In order to simplify the analysis, it is assumed that the pressure inside the liquid sheet is equal to the ambient pressure. A coordinate system is established on the injector axis symmetry plane; the center of the liquid sheet element is the origin, the radial velocity direction of the liquid sheet is the $r$ axis, and the normal direction outside the liquid sheet is the $n$ axis, as shown in Fig. 10.

Because the liquid sheet angle $\theta$ changes slightly when the liquid sheet moves closer to, and away from, the recess chamber wall within a period, the curvature in the $n$ direction approximates to infinity, and the effects of the centrifugal force $C_n$ in the $n$ direction and the surface tension $S_n$ are small. Thus, they are ignored. The centrifugal force $C_r$ and the surface tension $S_r$ in the $r$ direction are respectively calculated as follows:

$$C_r=\rho_l\omega^2(r)\,h(r)\cos\theta\frac{\mathrm{d}S}{r}, \tag{1}$$

$$S_r=2\sigma\frac{\mathrm{d}S}{r}, \tag{2}$$

where $\rho_l$ is the liquid density, $\omega(r)$ is the circumferential rotation speed of the liquid sheet, $r$ is the radial displacement, $h(r)$ is the thickness of the liquid sheet, d$S$ is the area of the liquid sheet element, and $\sigma$ is the surface tension coefficient, which is 0.073 for air and water.

The pressure outside the liquid sheet in the recess chamber can be calculated by the gas mass flow rate and the gas Mach number. The gas mass flow rate is calculated as

$$\dot{m}_g=\begin{cases}C_dA(r)P\sqrt{\dfrac{2k\left(\left(\dfrac{p_e}{P}\right)^{\frac{2}{k}}-\left(\dfrac{p_e}{P}\right)^{\frac{k+1}{k}}\right)}{(k-1)RT_g}}, & \sigma_{cr}<\dfrac{p_e}{P}\leqslant 1,\\ C_dA(r)P\sqrt{\dfrac{k}{RT_g}\left(\dfrac{2}{k+1}\right)^{\frac{k+1}{k-1}}}, & \dfrac{p_e}{P}\leqslant\sigma_{cr},\end{cases} \tag{3}$$

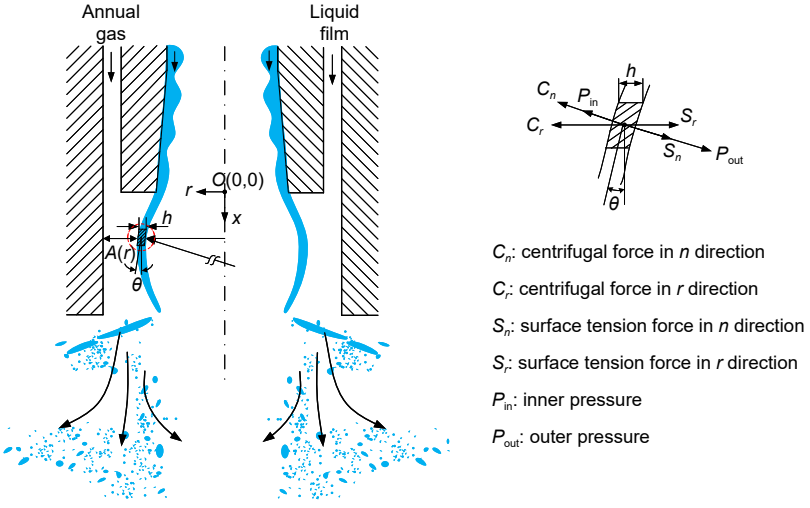


**Fig. 10 Force analysis of the liquid sheet element**

where the critical pressure ratio is $\sigma_{cr}=\left(\frac{2}{k+1}\right)^{\frac{k}{k-1}}$, $p_e$ is the ambient gas pressure, $P$ is the total pressure of the gas, $T_g$ is the total temperature of the gas, $R$ is the gas constant, $A(r)$ is the circulation area of the gas at the position of the liquid sheet, $k$ is the specific heat ratio, and $C_d$ is the gas flow coefficient.

There are three situations for calculating the circulation area of the gas: internal mixing, critical mixing, and external mixing. The range of self-pulsation is the largest in the internal mixing state, so the theoretical analysis model first considers that the injector is in internal mixing state, the liquid sheet does not contact the recess chamber wall, and when the liquid sheet element moves to the nearest wall of the recess chamber, the gas Mach number at this position is 1. Based on that, the circulation area is calculated as follows:

$$A(r)=\frac{1}{4}\pi D_{g,or}^2-\pi\left(r+\frac{h(r)}{2}\right)^2. \tag{4}$$

According to the gas mass flow rate formula, the relationship between the total pressure $P$ and the radial displacement $r$ of the liquid sheet is calculated as

$$P=\begin{cases}\left(\dfrac{p_e^{\frac{k-1}{k}}}{2}\pm\sqrt{\dfrac{\Delta^2}{p_e^{\frac{2}{k}}}+\dfrac{\left(p_e^{\frac{k-1}{k}}\right)^2}{4}}\right)^{\frac{k}{k-1}}, & \sigma_{cr}<\dfrac{p_e}{P}\leqslant 1,\\ \dfrac{\dot{m}_g}{C_d A(r)\sqrt{\dfrac{k}{RT_g}\left(\dfrac{2}{k+1}\right)^{\frac{k+1}{k-1}}}}, & \dfrac{p_e}{P}\leqslant\sigma_{cr},\end{cases} \tag{5}$$

where $\Delta=\dot{m}_g\Big/\left(C_d A(r)\sqrt{\dfrac{2k}{(k-1)RT_g}}\right)$.

Thus, the gas static pressure $p_{out}(r)$ and the gas injection speed $u_g$ can be solved by the isentropic relation, as follows:

$$p_{out}(r)=\frac{P}{\left(1+\dfrac{k-1}{2}M^2\right)^{\frac{k}{k-1}}}, \tag{6}$$

$$u_g=\begin{cases}\sqrt{\dfrac{2kRT_g}{k+1}}, & \dfrac{p_e}{P}\leqslant\sigma_{cr},\\ \sqrt{\dfrac{2kRT_g}{k-1}\left(1-\left(\dfrac{p_e}{P}\right)^{\frac{k-1}{k}}\right)}, & \sigma_{cr}<\dfrac{p_e}{P}\leqslant 1.\end{cases} \tag{7}$$

Then, the gas Mach number $M$ is calculated as:

$$M=\begin{cases}\sqrt{\dfrac{2T_g}{(k-1)T_s}\left(1-\left(\dfrac{p_e}{P}\right)^{\frac{k-1}{k}}\right)}, & \sigma_{cr}<\dfrac{p_e}{P}\leqslant 1,\\ \sqrt{\dfrac{2T_g}{(k+1)T_s}}, & \dfrac{p_e}{P}\leqslant\sigma_{cr},\end{cases} \tag{8}$$

where $T_s$ is the static temperature. The relationship between $T_g$ and $T_s$ satisfies the following equation:

$$\frac{T_g}{T_s}=1+\frac{M^2(k-1)}{2}. \tag{9}$$

Therefore, the gas Mach number can be simplified as follows:

$$M=\begin{cases}\sqrt{\dfrac{2\left(1-\left(\dfrac{p_e}{P}\right)^{\frac{k-1}{k}}\right)}{(k-1)\left(\dfrac{p_e}{P}\right)^{\frac{k-1}{k}}}}, & \sigma_{cr}<\dfrac{p_e}{P}\leqslant 1,\\ 1, & \dfrac{p_e}{P}\leqslant\sigma_{cr}.\end{cases} \tag{10}$$

The thickness $h(r)$ of the liquid sheet, the circumferential velocity $\omega(r)$ of the liquid sheet, the radial velocity $v(r)$ of the liquid sheet, and the liquid sheet angle $\theta$ in the recess chamber can be respectively solved by the conservation of mass, angular momentum, and energy, as follows:

$$h(r)=\frac{\dot{m}_l}{\rho_l u_0\cdot 2\pi r}, \tag{11}$$

$$\omega(r)=\frac{\omega_0\left(r_0-\dfrac{h_0}{2}\right)}{r}, \tag{12}$$

$$v(r)=\sqrt{v_0^2+\omega_0^2-\left(\frac{\omega_0\left(r_0-h_0/2\right)}{r}\right)^2}, \quad (13)$$

$$\cos\theta=\sqrt{\frac{1}{1+\left(\frac{v(r)}{u_0}\right)^2}}, \quad (14)$$

where $u_0$ is the initial axial velocity of the liquid sheet, $v_0$ is the initial radial velocity of the liquid sheet, $\omega_0$ is the initial circumferential velocity of the liquid sheet, $h_0$ is the initial thickness of the liquid sheet, and $r_0$ is the initial position of the liquid sheet element.

According to the force analysis, the resultant force $F$ of the liquid sheet element in the radial direction is obtained as follows:

$$F=\frac{\left(p_{\text{in}}-p_{\text{out}}(r)\right)\mathrm{d}S}{\cos\theta}-\frac{\rho_1\omega^2(r)\,h(r)\cos\theta\mathrm{d}S}{r}-\frac{2\sigma\mathrm{d}S}{r}, \quad (15)$$

where $p_{\text{in}}$ is the gas pressure inside the liquid sheet in the recess chamber, which is approximately equal to the environmental pressure $p_e$.

Therefore, the acceleration of the liquid sheet element is as follows:

$$\frac{\mathrm{d}^2r}{\mathrm{d}t^2}=\frac{p_{\text{in}}-p_{\text{out}}(r)}{\rho_1 h(r)(\cos\theta)^2}+\frac{\omega^2(r)}{r}-\frac{2\sigma}{\rho_1 h(r)\,r\cos\theta}. \quad (16)$$

This completes the establishment of the 1D self-pulsation model. The initial conditions, namely $u_0$, $v_0$, $\omega_0$, $h_0$, and $r_0$, can be solved by the theoretical model of the liquid sheet angle established by Bai (2020). Therefore, only the gas and liquid mass flow rates and the injector structure need to be known to obtain the time series of the liquid sheet movement position, the time series of the gas pressure outside the liquid sheet in the recess chamber, and the self-pulsation frequency and intensity.

The theoretical deviation of the calculated self-pulsation frequencies before and after the break phenomenon with the experimental self-pulsation frequencies is found to be less than 9%, as shown in Fig. 11. Therefore, the credibility of the model was verified. However, the self-pulsation model is incapable of determining whether self-pulsation occurs.

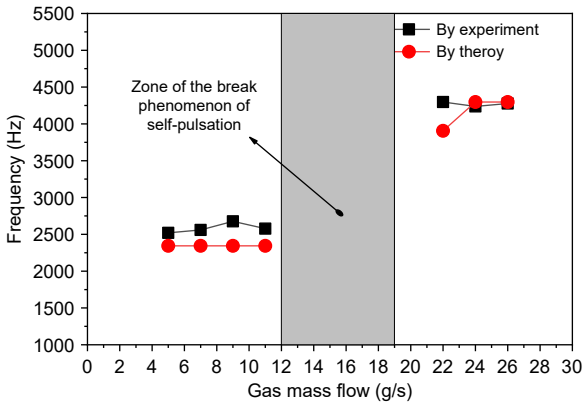


**Fig. 11 Relationship between the experimental and theoretical self-pulsation frequencies ($\dot{m}_l$=160 g/s)**

Fig. 12 presents the theoretical calculations of the time series of the movement positions of the liquid sheet in the recess chamber before and after the break phenomenon of self-pulsation, as well as the pressure outside the liquid sheet in the recess chamber.

After the occurrence of self-pulsation, the liquid sheet element in the recess chamber moves periodically. Before the break phenomenon of self-pulsation ($J$=3.14), the liquid sheet element first approaches, but does not reach, the recess chamber wall. With the decrease of the radial velocity of the liquid sheet element to zero, the distance between the liquid sheet element and the recess chamber wall is 0.4 mm, after which the liquid sheet element reverses to 1.3 mm away from the centerline. Under this working condition, the amplitude of the movement of the liquid sheet element is 2.8 mm (Fig. 12a), and the calculated peak pressure of the liquid sheet outside the recess chamber is 210 kPa (Fig. 12b). After the break phenomenon of self-pulsation ($J$=12.48), the liquid sheet element first weakly approaches the recess chamber wall, and then immediately moves toward the centerline of the injector. Under this working condition, the amplitude of the movement of the liquid sheet element is 2 mm (Fig. 12a), and the decrease of the amplitude reduces the peak and amplitude of the gas pressure outside the liquid sheet in the recess chamber (Fig. 12b). The transformation in the radial position of the liquid sheet element is the same as that of the liquid sheet flow pattern obtained by experiment.

Fig. 13 exhibits the relationship between the momenta of the gas and liquid phases under different working conditions. The gas- and liquid-phase momenta change periodically and have the same period, but the

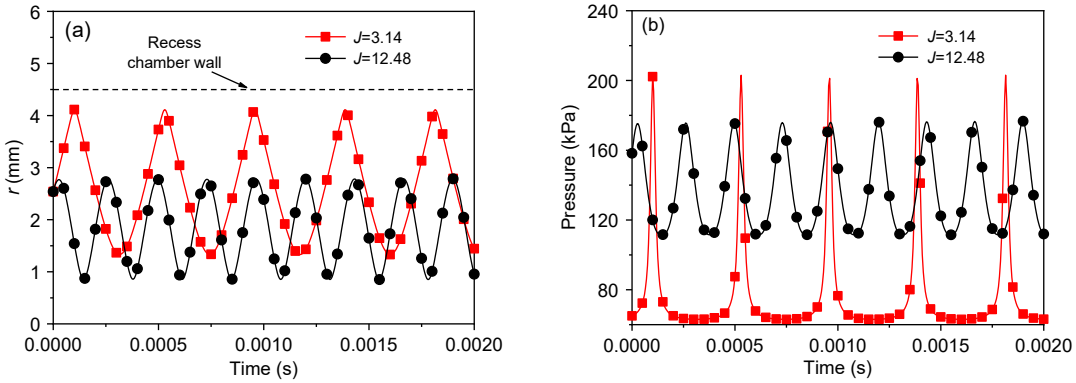


**Fig. 12 Time series of the radial position of the liquid sheet element (a) and the pressure outside the liquid sheet (b) in the recess chamber (by the theoretical model)**

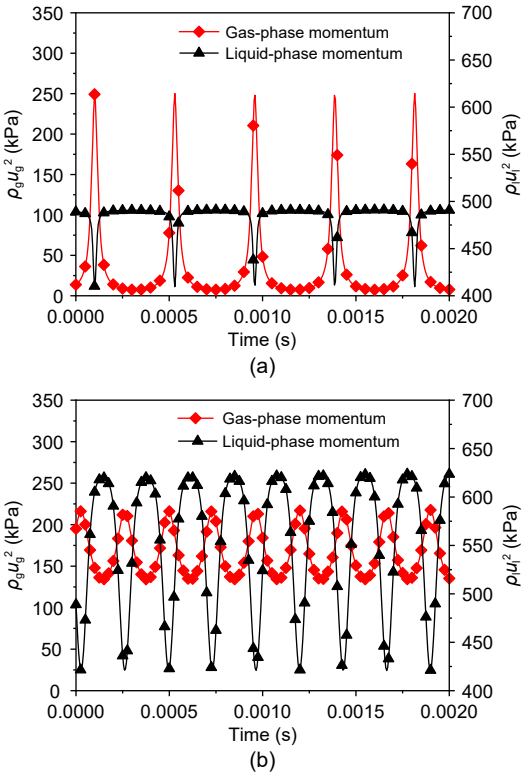


**Fig. 13 Time series of the momenta of the gas and liquid phases (by the theoretical model): (a) $J$=3.14; (b) $J$=12.48. $\rho_g u_g^2$ is the gas-phase momentum, and $\rho_l u_l^2$ is the liquid-phase momentum**

phase difference is $T/2$. Therefore, in the same period, the peaks of the momenta of the gas and liquid phases appear alternately (Fig. 13a), and the energies of the gas and liquid phases are periodically transferred to each other to maintain the self-pulsation. In general, the liquid-phase momentum is greater than the gas-phase momentum both before and after the break phenomenon of self-pulsation. This is because only a portion of the liquid-phase momentum is used to transfer energy to amplitude of the gas-phase momentum oscillation of self-pulsation after the break phenomenon is decreased (Fig. 13b), while that of the liquid-phase momentum is increased. This is because the gas mass flow rate is higher after the break phenomenon of self-pulsation; while the gas-phase owns a higher momentum, the liquid-phase momentum is nearly unchanged. Therefore, the energy transferred from the gas phase to the liquid phase within a cycle is greater, while the energy transferred from the liquid phase to the gas phase is relatively little.

## 4 Conclusions

Experimental investigations of the break phenomenon of self-pulsation, self-pulsation characteristics before and after the break phenomenon, and flow dynamics in the recess chamber generated by a LCSC injector under different $J$ conditions have been presented and analyzed. Moreover, a theoretical model for self-pulsation was proposed to analyze the oscillation characteristics of the liquid sheet during self-pulsation. The critical conclusions of the present study are as follows.

1. As the momentum flux ratio ($J$) increases, the break phenomenon of self-pulsation for the LCSC injector with a larger recess length occurs. The self-pulsated spray is more symmetric before the break phenomenon, and the turbulence of the spray is greatly strengthened, leading to an asymmetric distribution of the spray after the break phenomenon. When the break phenomenon of self-pulsation occurs, the gas-liquid

shear layer is relatively stable and the spray cone angle remains almost constant.

2. The flow dynamics in the recess chamber sequentially transform from a periodic expansion dominated flow to a stable flow, and then develop to a periodic contraction-dominated flow during the break process of self-pulsation. Before the break phenomenon, the liquid sheet has little effect on the pressure disturbance propagation speed in the recess chamber. After the break phenomenon, the pressure disturbance propagation speed is obviously affected by the liquid sheet. There is a 12% phase difference between the pressure time series of the two monitoring points.

3. Based on the theoretical analysis of the 1D unsteady flow process of the liquid sheet, it is preliminarily proved that the self-sustaining mechanism of self-pulsation changes from the periodic blockage of the conical liquid film before the break phenomenon to the periodic squeezing effect of the annular gas after the break phenomenon, and the self-pulsation frequency can be better predicted. Moreover, the energy transfers between the gas- and liquid-phase play a key role in maintaining the self-pulsation process.

## Acknowledgments

This work is supported by the National Natural Science Foundation of China (No. 11872375) and the National Science Foundation for Young Scientists of China (Nos. 11802323, 11902351, and 12102462).

## Author contributions

Peng-jin CAO designed the research. Peng-jin CAO and Xiao BAI processed the corresponding data. Peng-jin CAO wrote the first draft of the manuscript. Xiao BAI helped to organize the manuscript. Peng CHENG provided the methodology. Qing-lian LI revised and edited the final version.

## Conflict of interest

Peng-jin CAO, Xiao BAI, Qing-lian LI, and Peng CHENG declare that they have no conflict of interest.

## References

Ahn K, Kim JG, Choi HS, 2014. Effects of injector recess on heat flux in a combustion chamber with cooling channels. *Aerospace Science and Technology*, 37:110-116. https://doi.org/10.1016/j.ast.2014.05.012

Armbruster W, Hardi JS, Suslov D, et al., 2018. Experimental investigation of self-excited combustion instabilities with injection coupling in a cryogenic rocket combustor. *Acta Astronautica*, 151:655-667. https://doi.org/10.1016/j.actaastro.2018.06.057

Armbruster W, Hardi JS, Miene Y, et al., 2020. Damping device to reduce the risk of injection-coupled combustion instabilities in liquid propellant rocket engines. *Acta Astronautica*, 169:170-179. https://doi.org/10.1016/j.actaastro.2019.11.040

Bai X, 2020. The Self-Pulsation and Its Effects on Spray Combustion Characteristics for Gas-Liquid Swirl Coaxial Injector. National University of Defense Technology, Changsha, China (in Chinese).

Bai X, Li QL, Cheng P, et al., 2018. Investigation of self-pulsation characteristics for a liquid-centered swirl coaxial injector with recess. *Acta Astronautica*, 151:511-521. https://doi.org/10.1016/j.actaastro.2018.07.002

Bai X, Cheng P, Sheng LY, et al., 2019. Effects of backpressure on self-pulsation characteristics of liquid-centered swirl coaxial injectors. *International Journal of Multiphase Flow*, 116:239-249. https://doi.org/10.1016/j.ijmultiphaseflow.2019.04.017

Bai X, Sheng LY, Li QL, et al., 2020a. Effects of annulus width and post thickness on self-pulsation characteristics for liquid-centered swirl coaxial injectors. *International Journal of Multiphase Flow*, 122:103140. https://doi.org/10.1016/j.ijmultiphaseflow.2019.103140

Bai X, Cheng P, Li QL, et al., 2020b. Effects of self-pulsation on combustion instability in a liquid rocket engine. *Experimental Thermal and Fluid Science*, 114:110038. https://doi.org/10.1016/j.expthermflusci.2019.110038

Bai X, Cao PJ, Li QL, et al., 2021. The break phenomenon of self-pulsation for liquid-centered swirl coaxial injectors. *International Journal of Multiphase Flow*, 142:103708. https://doi.org/10.1016/j.ijmultiphaseflow.2021.103708

Bazarov VG, Yang V, 1998. Liquid-propellant rocket engine injector dynamics. *Journal of Propulsion and Power*, 14(5): 797-806. https://doi.org/10.2514/2.5343

Chen XD, Yang V, 2014. Effect of ambient pressure on liquid swirl injector flow dynamics. *Physics of Fluids*, 26(10): 102104. https://doi.org/10.1063/1.4899261

Chu W, Li XQ, Tong YH, et al., 2020. Numerical investigation of the effects of gas-liquid ratio on the spray characteristics of liquid-centered swirl coaxial injectors. *Acta Astronautica*, 175:204-215. https://doi.org/10.1016/j.actaastro.2020.05.050

Chu W, Ren YJ, Tong YH, et al., 2021. Numerical study of effects of backpressure on self-pulsation of a liquid-centred swirl coaxial injector. *International Journal of Multiphase Flow*, 139:103626. https://doi.org/10.1016/j.ijmultiphaseflow.2021.103626

Eberhart CJ, Frederick Jr RA, 2017a. Fluid oscillations of a swirl coaxial injector under high-frequency self-pulsation. *Journal of Propulsion and Power*, 33(4):804-814. https://doi.org/10.2514/1.b36177

Eberhart CJ, Frederick Jr RA, 2017b. Details on the mechanism of high-frequency swirl coaxial self-pulsation. *Journal of Propulsion and Power*, 33(6):1418-1427. https://doi.org/10.2514/1.B36216

Fu QF, Yang LJ, Qu YY, 2011. Measurement of annular liquid film thickness in an open-end swirl injector. *Aerospace Science and Technology*, 15(2):117-124. https://doi.org/10.1016/j.ast.2010.06.006

Giannadakis A, Naxakis A, Romeos A, et al., 2019. An experimental study on a coaxial flow with inner swirl: vortex evolution and flow field mixing attributes. *Aerospace Science and Technology*, 94:105373. https://doi.org/10.1016/j.ast.2019.105373

Gomet L, Robin V, Mura A, 2014. Lagrangian modelling of turbulent spray combustion under liquid rocket engine conditions. *Acta Astronautica*, 94(1):184-197. https://doi.org/10.1016/j.actaastro.2013.08.016

Huang YH, Zhou J, Hu XP, et al., 1998. Experiment and acoustic model for the self-oscillation of coaxial swirl injector and its influence to combustion of liquid rocket engine. *Acta Acustica*, 23(5):459-465 (in Chinese). https://doi.org/10.15949/j.cnki.0371-0025.1998.05.011

Im JH, Yoon Y, 2013. The effects of the ambient pressure on self-pulsation characteristics of a gas/liquid swirl coaxial injector. *Orthopedics & Traumatology*, 38(2):435-438. https://doi.org/10.2514/6.2013-4850

Im JH, Kim D, Han P, 2009. Self-pulsation characteristics of a gas-liquid swirl coaxial injector. *Atomization and Sprays*, 19(2):57-74. https://doi.org/10.1615/AtomizSpr.v19.i1.40

Kang ZT, Li QL, Cheng P, et al., 2016a. Effects of recess on the self-pulsation characteristics of liquid-centered swirl coaxial injectors. *Journal of Propulsion and Power*, 32(5):1124-1132. https://doi.org/10.2514/1.B35632

Kang ZT, Li QL, Cheng P, et al., 2016b. Effects of self-pulsation on the spray characteristics of gas-liquid swirl coaxial injector. *Acta Astronautica*, 127:249-259. https://doi.org/10.1016/j.actaastro.2016.05.038

Kang ZT, Wang ZG, Li QL, et al., 2018. Review on pressure swirl injector in liquid rocket engine. *Acta Astronautica*, 145:174-198. https://doi.org/10.1016/j.actaastro.2017.12.038

Kim D, Im JH, Koh H, et al., 2007a. Effect of ambient gas density on spray characteristics of swirling liquid sheets. *Journal of Propulsion and Power*, 23(3):603-611. https://doi.org/10.2514/1.20161

Kim D, Han P, Im JH, et al., 2007b. Effect of recess on the spray characteristics of liquid–liquid swirl coaxial injectors. *Journal of Propulsion and Power*, 23(6):1194-1203. https://doi.org/10.2514/1.30450

Kim JG, Han YM, Choi HS, et al., 2013. Study on spray patterns of gas-centered swirl coaxial (GCSC) injectors in high pressure conditions. *Aerospace Science and Technology*, 27(1):171-178. https://doi.org/10.1016/j.ast.2012.08.004

Kim YJ, Sohn CH, Hong M, et al., 2014. An analysis of fuel–oxidizer mixing and combustion induced by swirl coaxial jet injector with a model of gas–gas injection. *Aerospace Science and Technology*, 37:37-47. https://doi.org/10.1016/j.ast.2014.05.006

Li HX, Ye L, Wei XL, et al., 2017. The design and main performance of a hydrogen peroxide/kerosene coaxial-swirl injector in a lab-scale rocket engine. *Aerospace Science and Technology*, 70:636-643. https://doi.org/10.1016/j.ast.2017.09.003

Li QL, Kang ZT, Zhang XQ, et al., 2016. Effect of recess length on the spray characteristics of liquid-centered swirl coaxial injectors. *Atomization and Sprays*, 26(6):535-550. https://doi.org/10.1615/AtomizSpr.2015011831

Lux J, Haidn O, 2009. Effect of recess in high-pressure liquid oxygen/methane coaxial injection and combustion. *Journal of Propulsion and Power*, 25(1):24-32. https://doi.org/10.2514/1.37308

Ranade IS, Frederick RA, 2019. Experimental study of swirl coaxial injector hydrodynamics under high-frequency self-pulsation. Proceedings of the AIAA Propulsion and Energy 2019 Forum.

Ren YJ, Chu W, Tong YH, et al., 2021a. Numerical investigation on spray self-pulsation characteristics of a liquid-centered swirl coaxial injector. *Aerospace Science and Technology*, 112:106593. https://doi.org/10.1016/j.ast.2021.106593

Ren YJ, Guo KK, Zhao JF, et al., 2021b. Numerical investigation of spray self-pulsation characteristics of liquid-centered swirl coaxial injector with different recess lengths. *International Journal of Multiphase Flow*, 138:103592. https://doi.org/10.1016/j.ijmultiphaseflow.2021.103592

Yang LJ, Fu QF, 2011. Theoretical investigation on the dynamics of a gas-liquid coaxial swirl injector. *Journal of Propulsion and Power*, 27(1):144-150. https://doi.org/10.2514/1.B34004

Yang LJ, Ge MH, Zhang MZ, et al., 2008. Spray characteristics of recessed gas-liquid coaxial swirl injector. *Journal of Propulsion and Power*, 24(6):1332-1339. https://doi.org/10.2514/1.23977

Yuan L, Shen CB, 2016. Large eddy simulation of combustion instability in a tripropellant air heater. *Acta Astronautica*, 129:59-73. https://doi.org/10.1016/j.actaastro.2016.08.002